Dual-Frequency Electric–Magnetic–Electric Microstrip Leaky-Mode Antenna of a Single Fan Beam

Yu-Chiao Chen, *Student Member, IEEE*, Ching-Kuo Wu, *Student Member, IEEE*, and Ching-Kuang C. Tzuang, *Fellow, IEEE*

***Abstract*—This paper presents a dual-frequency electric–magnetic–electric (EME) microstrip exhibiting two leaky-wave regions of similar radiation characteristics like the microstrip EH_1 mode. The EME microstrip incorporates a photonic bandgap (PBG) structure, which is a two-dimensional array consisting of unit cell made of coupled coils connected by a via. The PBG structure employed in the EME prototype conducts at dc and shows the first stopband between 8.8–12.4 GHz, thus rendering the so-called magnetic surface. The EME microstrip is essentially made by substituting the PBG cells for the metal strip of a conventional microstrip. The finite-element method (FEM) analyses of the PBG structure show that the first and second modes are TM-like and TEM-like, respectively. The latter is leaky between 12.4–12.9 GHz and is found to be responsible for the second leaky region of the EME microstrip. The dispersion characteristics of the EME microstrip are obtained by two theoretical methods, namely, the matrix-pencil method and the FEM. Both show excellent agreement in the two leaky regions. Furthermore, the measured far-field radiation patterns of the two leaky regions also validate the dispersion curves. The first leaky region is of EH_1 type and between 5.05–5.45 GHz. The second leaky region radiates a frequency-scanning fan beam between 11.95–13.0 GHz, similar to those of the EH_1 mode. Detailed modal current analyses show even and odd symmetry along longitudinal and transverse plane of EME microstrip, respectively, further confirming the two leaky regions behave like the well-known EH_1 leaky mode. The proposed EME microstrip enriches the modal characteristics of the conventional, uniform microstrip and is thus a manifestation of application of PBG structure for new guiding device.**

***Index Terms*—Dual frequency, leaky-mode antenna, photonic bandgap (PBG).**

I. Introduction

PHOTONIC bandgap (PBG) structures are artificially engineered two- or three-dimensionally periodic structures. Although early research focused on the optical field [1], [2], PBG structures are readily scaleable and applicable to a broad range of frequencies, including those of microwaves and millimeter waves. Electromagnetic waves that propagate in artificial, multidimensional periodic structures resemble electron waves that propagate in natural crystals. These materials can prevent the omnidirectional propagation of electromagnetic waves within certain frequency bands and exhibit passbands and stopbands for either guided waves along transmission lines or surface waves in dielectric substrates [3]–[15]. PBG structures also exhibit two distinctive physical features. First, PBG structures typically consist of continuous metal and dc current conducted therein and can induce a magnetic surface (MS) at a forbidden frequency band. In the stopband, the tangential magnetic field is weak, even with a large electric field along the surface, and the surface impedance is very high. Such a structure is occasionally called a high impedance surface or an MS. In contrast to normal conductors, a high impedance surface can effectively suppress the propagation of surface waves and reflect electromagnetic waves without reversing their phase [5], [6]. Second, PBG cells or periodic devices latticed on the ground plane of a microstrip structure exhibit great versatility in controlling the dispersion characteristics of electromagnetic waves. Not only does the passband forbid wave propagating in the stopband, but the passband of the microstrip PBG structures display the slow-wave effect and has been used to reduce the dimensions of circuits. Moreover, the broad stopband characteristics have been applied to effectively suppress spurious transmission in the passband of filters and leakage from guided-wave structures [7]–[9]. The feasibility of applying PBG phenomena to both the optical and the microwave/millimeter-wave domains for industrial use has been extensively investigated [3]–[15]. PBG structures have attracted much interest among microwave engineers, primarily owing to their potential applications in several important areas such as microwave antennas, compact spurious-free filters, and frequency-selective surfaces (FSSs). For example, a uniplanar compact photonic bandgap (UC-PBG) structure was invented and its applications have proliferated in various fields of microwave engineering [6]–[10]. The gain of a microstrip antenna can be considerably increased by using a PBG layer as a substrate or by latticing PBG cells on the ground plane [8], [12]. A high impedance ground plane has been developed using metal plates with vertical vias [5].

Instead of latticing PBG cells on the ground plane of the microstrip structure, we place new PBG cells on the signal line to develop a new microstrip structure. This microstrip structure maintains the slow-wave effect and stopband characteristics. The dispersion characteristics of the PBG structure could be adjusted through changing the cell numbers along the transverse plane on the strip or tuning the dimensions of the PBG cells. The new PBG cells exhibit a high-impedance-surface state

Manuscript received April 6, 2002; revised August 21, 2002. This work was supported by the Ministry of Education of Taiwan under Grant 89-E-FA06-2-4, and by the National Science Council under Grant NSC 91-22213-E-009-063.

The authors are with the Institute of Electrical Communication Engineering, National Chiao Tung University, Hsinchu, Taiwan, R.O.C. (e-mail: cktzuang@cc.nctu.edu.tw).

Digital Object Identifier 10.1109/TMTT.2002.805201

0018-9480/02$17.00 © 2002 IEEE

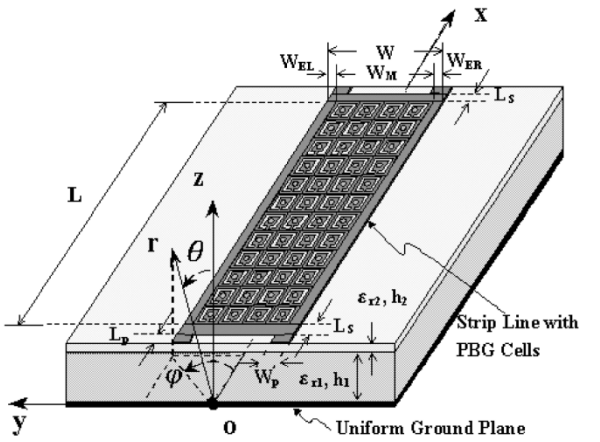

(a)

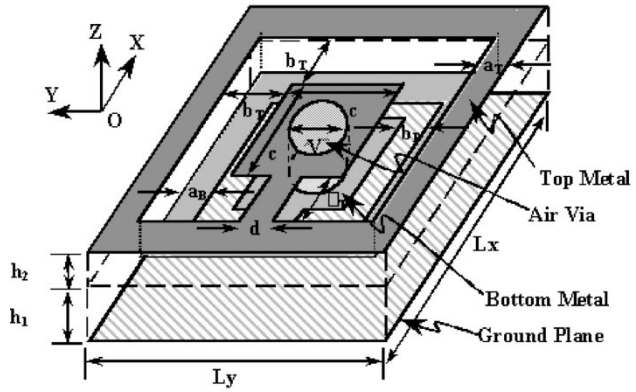

(b)

Fig. 1. EME microstrip. (a) EME transmission line. $h_1 = 0.508$ mm, $\varepsilon_{r1} = 3.38$, $h_2 = 0.203$ mm, $\varepsilon_{r2} = 3.38$, $W_{\rm EL} = W_{\rm ER} = 0$ mm, $W_M = W = 8.536$ mm, $W_P = 1.6$ mm, $L_S = 0.5$ mm, and $L = 256$ mm. (b) Unit cell incorporated in the MS. $h_1 = 0.508$ mm, $h_2 = 0.203$ mm, $Lx = Ly = 2.134$ mm, $a_T = 0.127$ mm, $b_T = 0.508$ mm, $c = 0.864$ mm, $d = a_B = b_B = 0.254$ mm, and $V = 0.406$ mm.

in a certain frequency band and behave like an MS by reflecting the incoming electromagnetic wave without reversing its phase. Electric surface and MS alternate transversely on the signal line, thus forming an electric–magnetic–electric (EME) microstrip, as shown in Fig. 1(a). Fig. 1(b) shows the expanded view of the unit cell incorporated in the EME microstrip. Detailed design information of the unit cell is available in [9]–[11]. The unit cell consists of a high-impedance surface made of coupled inductors connected by a via, a substrate of thickness 0.203 mm and relative dielectric constant of 3.38, and a conducting uniform ground plane. The EME microstrip exhibits low-loss slow-wave bound mode propagation [9], [10]. The dispersion characteristics of the EME microstrip at zeroth order and first order, named the bound EH_0 and leaky EH_1 modes, have been reported in [11]. A reduced-size EME parallel coupled band-pass filter with suppressed spurious responses had been reported in a very similar way to the filter made of coupled microstrips on UC-PBG ground plane [7], [9].

Replacing the signal strip by the proposed PBG cells, the propagation characteristics of EME microstrip are enriched by the additional degrees of freedom offered by the PBG cells. As will become clearer in Section II, the two-dimensional (2-D) PBG cell incorporated in our design shows unisotropic properties with the lowest order TM-like mode, followed by a stopband, and the first higher order TEM-like mode as frequency increases. The lowest order TM-like mode is bound and begins at dc with a slow-wave factor greater than $\sqrt{\varepsilon_r}$, where ε_r is the relative dielectric constant of the substrate between the high impedance surface and the uniform ground plane. Consequently, the onset frequency of the EH_1 mode of the EME line is much lower than that of a conventional, uniform microstrip of the same width [11]. This is the first leaky EH_1 mode exhibiting a fan beam with frequency-scanning characteristics. Such an EH_1 leaky mode can be excited by an out-of-phase differential signal at the opposite ends of the EME microstrip [16]. The same differential feeds can also excite the first higher order TEM-like mode of the PBG cells at higher frequencies, rendering a dual-frequency scanning leaky-mode antenna with a single fan beam for the first time.

The prototype presented in this paper, although not optimized to specific frequencies, is aimed at demonstrating the feasibility of using the EME microstrip as a dual-frequency leaky-mode antenna, with similar frequency scanning and fan beam characteristics. Section II reports the dispersion characteristics of the PBG unit cell which are important for designing and understanding the dual-frequency EME leaky-mode antenna. Section III reports the design principle of the EME leaky-mode microstrip antenna and dispersion characteristics at higher orders. An experiment is performed to validate the reported numerical results and to present the attractive features of the EME microstrip. Conclusions are finally made in Section IV.

II. Dispersion Diagram of Unbounded 2-D PBG Cells

The geometry and characteristic dimensions of the recently developed PBG cell, latticed on the strip line of the EME microstrip shown in Fig. 1(a), are sketched in Fig. 1(b). The unisotropic PBG cell has coupled spiral coils on both sides of a printed RO4003 substrate of thickness (h_2) 0.203 mm and relative permittivity (ε_r) 3.38, and connected by the center metal via through this thin substrate. In the design presented here, the unit cell is 2.134-mm wide (Lx or Ly) in both the x and y directions. The PBG cells are connected to adjacent cells on the top layer. More detailed information about the PBG unit cell is available in the caption of Fig. 1.

To investigate the propagation and stopband characteristics of the PBG cells incorporated in the EME microstrip, the theoretical dispersion diagram of the unbounded 2-D PBG periodical structure with unit cell shown in Fig. 1(b) is obtained by invoking the finite-element method [8]. Fig. 2 shows the dispersion diagram tracing along three sides of the irreducible Brillouin zone (BZ) triangle, as indicated in the inset of Fig. 2. The straight solid line and dashed line, referred to as the air-filled TEM line and the dielectric-filled TEM line, respectively, represent TEM wave propagations in free space and in a dielectric material of relative permittivity of 3.38, respectively. The first mode in dotted symbols deviates from the dashed line up to a certain frequency and then becomes relatively flat. Fig. 3(a) and (b) plots the electric field and magnetic field of

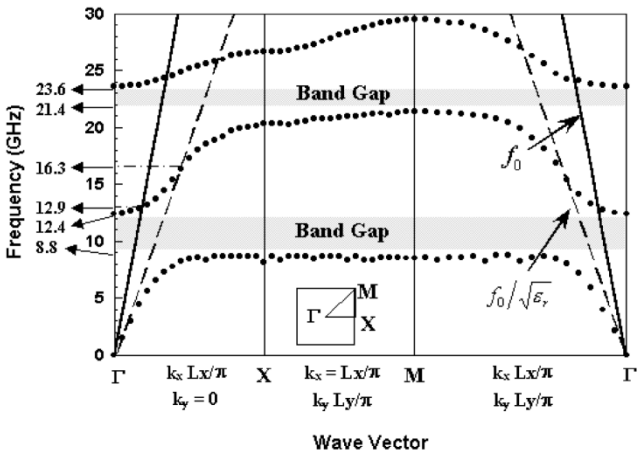

Fig. 2. Dispersion diagram of the MS using the unit cell of Fig. 1(b). Lx and Ly denote the lengths of the PBG unit cell in the x and y directions, respectively. k_x and k_y denote the wave numbers of the PBG unit cell in the x and y directions, respectively.

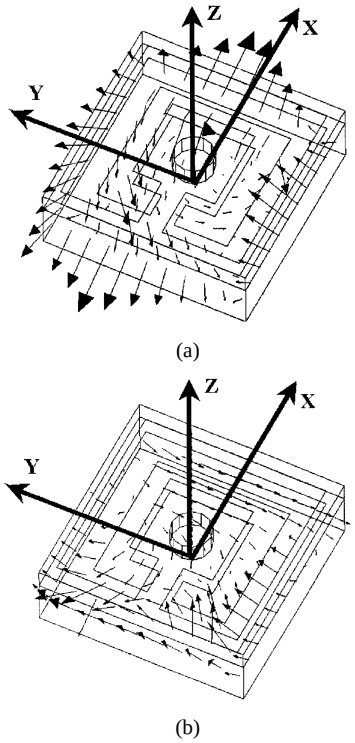

(a)

(b)

Fig. 3. TM-like mode at the X point of the BZ. (a) Electric field. (b) Magnetic field.

the X point of the BZ (see Fig. 2) below the top metal coils at $z = 0.25$ mm, respectively, showing that the first mode is predominantly a TM mode. The electric field of the first mode has strong components along the longitudinal direction of the wave propagation and localized at the edge of the PBG unit cells in the x direction; the magnetic field has a major component transverse to the propagation direction. Notice that the x axis of the PBG cell coincides with the longitudinal direction of EME microstrip as seen in Fig. 1(a) and (b). The second mode begins at 12.4 GHz and crosses the air-filled TEM line at 12.9 GHz. Between 12.4–12.9 GHz, the second mode leaks in the forward direction with an angle from broadside to horizon as frequency increases. Fig. 4(a) and (b) plots the electric and magnetic

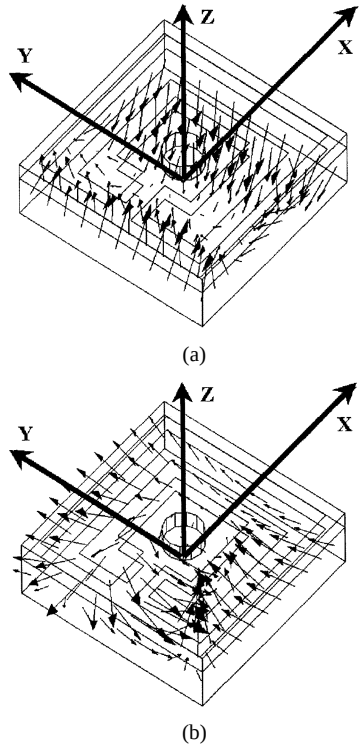

(a)

(b)

Fig. 4. TEM-like mode at the X point of the BZ. (a) Electric field. (b) Magnetic field.

fields of the X point of the BZ at $z = 0.25$ mm, indicating that the second mode is predominantly a TEM mode, since both electric and magnetic fields are predominantly perpendicular to the direction of wave propagation. The second mode has strong electric field components in the z direction and magnetic field components mainly along the y direction. The TEM mode, after crossing the air-filled TEM line and before entering the dielectric-filled TEM line, becomes leaky in the surface. When the frequency is higher than 16.3 GHz, the TEM surface leaky wave becomes a bound mode and reaches the second stopband near 21.4 GHz. A complete bandgap exists between the first and second modes, which spans the frequency range from 8.8 to 12.4 GHz, and a second narrower stopband could be observed between the second and third modes, centered at 22.5 GHz and spanning from 21.4 to 23.6 GHz.

III. Dual-Frequency EME Leaky-Mode Antenna

A. Design and Operational Principle

A short EME microstrip prototype with $W_M = 8.536$ mm ($W_{\mathrm{EL}} = W_{\mathrm{ER}} = 0$ mm) and $L = 32$ mm, with approximately one EH_0 guided wavelength at 5.25 GHz, is considered. A metal strip with the same width ($W_M = 8.536$ mm), but 0.5-mm long ($L_S = 0.5$ mm) is added to each end of the EME microstrip to facilitate the connection to the feeding structure. The small uniform microstrip feed line, at one of the four corners of Fig. 1(a), is 1.6-mm wide ($W_p = 1.6$ mm) and 0.5-mm long ($L_p = 0.5$ mm) and acts as a 50-Ω microstrip on the combined substrates.

A conventional microstrip leaky line is fed with an out-of-phase differential signal, and the first higher order leaky mode is appropriately excited. The differential feed is also applied to

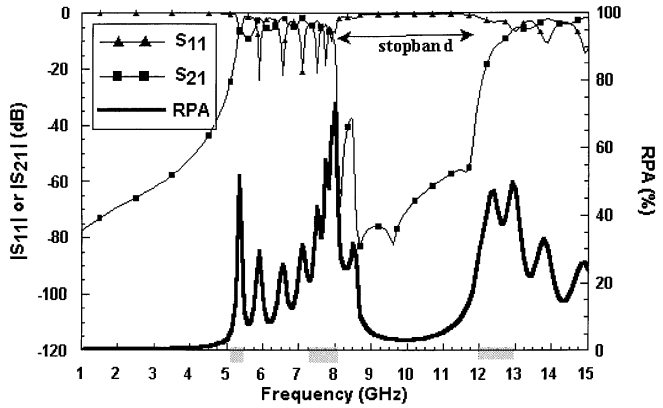

Fig. 5. Theoretical two-port scattering parameter and RPA value of the EME microstrip under differential excitations.

the EME microstrip, similarly. Proper widths ($W_{\rm EL}$, $W_{\rm ER}$, and W_M) of the electric surfaces and MSs can be selected to obtain the required propagation constants and the useful operating frequencies of the leaky-mode antenna. A special EME microstrip, referred to as an MS microstrip, filled with PBG cells on the strip of the EME microstrip ($W_{\rm EL} = W_{\rm ER} = 0$ mm) is applied in our work. The width of the EME microstrip incorporated in the prototype is 47.5% less than that of a uniform microstrip leaky-wave antenna, which is 16.256 mm at the same 5.45-GHz onset frequency [11]. Below 5.45 GHz, the onset frequency of the EH_1 mode of the EME microstrip, the first leaky EH_1 mode is excited and the EME microstrip antenna can radiate with a single frequency-scanning fan beam, like a conventional microstrip leaky-wave antenna [11].

Increasing the operating frequency to around 12.4 GHz (the upper corner of the first complete stopband of the PBG MS shown in Fig. 2) excites the TEM mode of the PBG cell without changing the feeding structure of the EME microstrip. The TEM mode of the PBG MS induces the second leaky mode of the EME microstrip and radiates in the forward direction between 12.4–12.9 GHz (see Fig. 2). As will become clearer in the following descriptions, the current distribution of the second leaky mode of the EME microstrip resembles the current distribution of the conventional microstrip leaky-wave antenna. In contrast to the second or third higher order leaky modes of the uniform microstrip with multiple beams, the second leaky mode of the EME microstrip radiates with a single fan beam. Thus, a dual-frequency EME microstrip antenna can be designed with frequency-scanning and single fan beam properties.

Notice that the number of PBG cells in the transverse direction of the EME microstrip should be large enough to apply the BZ dispersion data, which assumes that the PBG MS is infinite. In the EME prototype of Fig. 1, four cells will be shown to be adequate to emit the second leaky mode near 12.4 GHz.

Theoretical scattering analyses of the short EME microstrip are first conducted using differential excitations. Fig. 5 presents the theoretical results obtained by a commercial full-wave integral equation solver IE3D. The radiation efficiency of the EME microstrip can be estimated by the expression for the relative power absorbed (RPA), which is $1 - |S_{11}|^2 - |S_{21}|^2$ [17]. The value of the relative power absorbed (RPA) represents the total power losses of the electromagnetic device under investigation. The losses may include radiation loss, metal loss, dielectric loss, and surface-wave loss. Notably, neither the conductor loss nor the dielectric loss are separated from the leakage power in the RPA calculation. Additionally, the losses and the leakage power are much weaker than those of the experimental EME microstrip antenna, because the RPA calculation considers the EME microstrip prototype with only one guided wavelength. The RPA value is an approximate measure of the antenna radiation efficiency and provides an additional viewpoint to investigate the properties of the EME microstrip. Between 8.1–11.9 GHz, the reflection coefficient is almost unity and the RPA value is less than 10%, forming a stopband. The stopband closely correlates to the first complete forbidden band of the dispersion diagram from 8.8 to 12.4 GHz. The RPA results show that three peak regions have RPA values greater than 30%, wherein much energy is lost. The frequency of the first peak of the RPA value is approximately 5.35 GHz, consistent with the design of the EME microstrip antenna with the 5.45-GHz onset frequency [11]. The PBG structure could reduce the significant crosstalk or transmission in the stopband, but a considerable amount of coupling or crosstalk is consistently presented in the passband, especially at the corner of the stopband. The second peak of the RPA value, at around 8 GHz, is near the lower corner of the stopband of the EME microstrip, and energy vanishes due to the surface wave loss [18]. The third peak region appears between 12.1–13.1 GHz, very close to the TEM leaky wave region of the dispersion diagram of Fig. 2.

Closely examining the current distributions on the ground plane at $z = 0$ mm provides valuable physical information concerning the behavior of the EME microstrip at higher orders, such as the dispersion characteristics of the modes. Fig. 6(a) shows the current distributions on the ground plane of the EME microstrip excited differential at the left-hand side while the right-hand side port is terminated by a 50-Ω load at 5.25 GHz. The current vectors are primarily transverse to the direction of the waves that propagate along the EME microstrip. Fig. 6(b) plots the current distribution on the ground plane of the EME microstrip line at 12.35 GHz. In both leaky regions, the currents vectors on the ground plane of the EME microstrip are primarily transverse to the direction of the waves that propagate along the EME microstrip.

B. Dispersion Characteristics of EME Microstrip at Higher Orders

The excited surface currents at the ground plane ($z = 0$ mm) of the EME microstrip record the information of the space harmonics [19]–[21]. The excited electromagnetic wave components that propagate on the EME microstrip are the superposition of space harmonics due to the presence of a periodic PBG. The space harmonic component is denoted by its complex propagation constant $\gamma^{\pm}_{m,n}(\alpha^{\pm}_{m,n} + j\beta^{\pm}_{m,n})$, which represents a traveling-wave component of the nth higher order space component associated with the microstrip EH_m mode: the superscript $+$ ($-$) signifies the forward- (backward-) traveling-wave components. In the matrix-pencil method [22], [23], a number of significant decimal digits provides a sanity check during the noise-eliminating process. Four significant digits applied in our analyses of the particular EME microstrip indicate that the am-

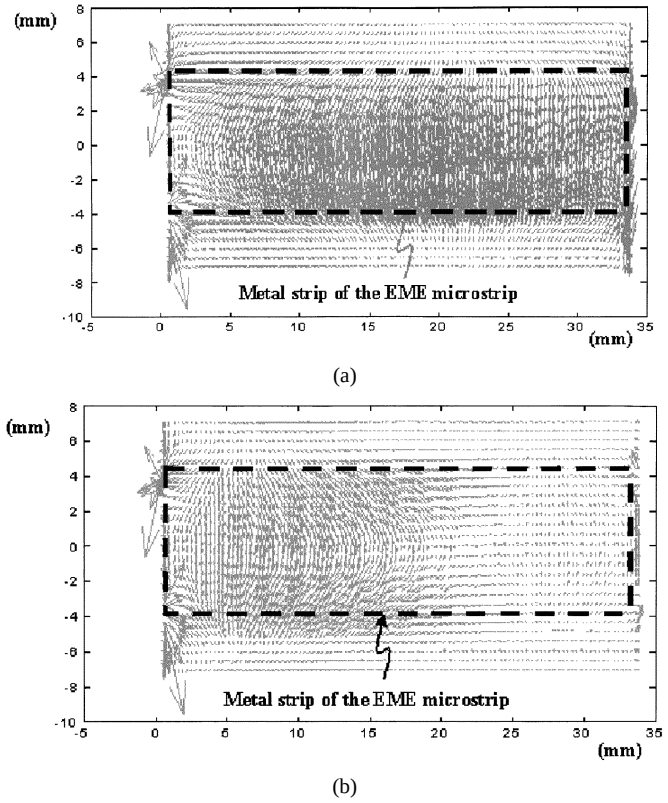

Fig. 6. Current distribution on the ground plane of the EME microstrip ($z = 0$ mm). The dashed rectangle indicates the position of the metal strip of the EME microstrip. (a) At 5.25 GHz. (b) At 12.35 GHz.

plitudes of the higher order space harmonics ($n > 0$) are approximately less than 1% of the amplitude of the dominant space harmonic ($n = 0$), both in the forward and the backward directions. Therefore, a forward traveling wave, represented by the complex propagation constant $\gamma_{1,0}^{+}$, and a backward traveling wave, denoted by $\gamma_{1,0}^{-}$, are the two major wave components between 4 –14 GHz. Both $\gamma_{1,0}^{+}$ and $\gamma_{1,0}^{-}$ have the same magnitude, but opposite signs. Outside this frequency range, only the forward traveling wave $\gamma_{1,0}^{+}$ contributes markedly to the total field because of the high attenuation constant.

Fig. 7 presents the normalized propagation constant of the forward traveling-wave component for the EME microstrip. The solid line represents the normalized phase constant and the dashed line represents the normalized attenuation constant. Below the first onset frequency at 5.45 GHz, the first higher order EH_1 mode leaks, and its attenuation constant increases with a decreasing frequency. Therefore, the EME microstrip radiates between 5.05–5.45 GHz, as shown in Fig. 5. The second leaky region could be observed between approximately 12.0–13.0 GHz, which closely correlates to the leaky-wave region of the second TEM mode of the PBG MS of Fig. 2 and the peaked RPA region of Fig. 5. Above 5.45 GHz, the normalized phase constant is in excess of unity, as frequency is increased toward 8.0 GHz. If the frequency is increased further over 8 GHz, then the propagation constant becomes complex again, with a decreasing normalized phase constant and changing normalized attenuation constant between 8–12 GHz, until the curve again enters a leaky region, wherein a fast wave propagates with a complex propagation constant. However, the

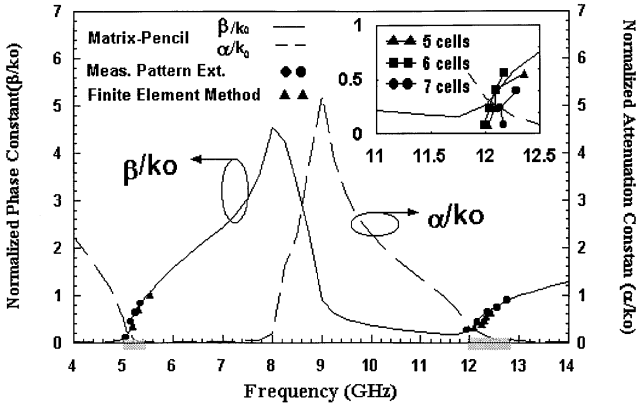

Fig. 7. Normalized phase constant β/k_0 and normalized attenuation constant α/k_0 of the leaky mode of the EME microstrip propagating in the forward direction.

leaky mode is not easily excited in this region because of high normalized attenuation constant ($\alpha/k_0 \succ 1$). These findings closely correspond to the scattering analyses shown in Fig. 5.

Next, the finite-element HFSS is applied to confirm the theoretical results obtained by the matrix-pencil technique. The EME microstrip prototype, used in the finite-element method simulation, has four cells in the transverse direction and one cell in the longitudinal direction with the linked boundary condition (LBC) at the cell sidewalls to simulate periodicity. An open boundary transverse to the propagation direction can be modeled accurately by perfectly matched layers (PMLs). The normalized phase constants are given only in the radiation regions. Fig. 7 shows that excellent agreement is achieved for data obtained by the matrix-pencil and finite-element methods.

The inset of Fig. 7 exhibits the correlation between the numbers of the PBG cells, transverse to the longitudinal direction that waves propagate, and the position of the second radiation region. The solid lines with triangles, squares, and circles represent the normalized phase constants of the EME microstrip containing five PBG cells, six PBG cells, and seven PBG cells transverse to the propagation in the second radiation region. The inset shows that various curves are nearly the same in the leaky region of interest, although the EME microstrip with transverse cells greater than four is wider than the prototype. The EME microstrip with four cells along the transverse direction can exhibit the modal behavior of the infinite-periodic 2-D PBG array, shown in Fig. 2.

Fig. 8(a) presents the transverse and longitudinal modal currents obtained by the matrix-pencil method at 5.25 GHz. Currents are normalized to a maximum of unity. The central plane of the signal line latticed by the PBG cells is at $y = 0$ mm and the width $W_M = 8.536$ mm. Real and imaginary parts of the longitudinal current (J_x) are odd-symmetric and have null values on the central x–z plane. Real and imaginary parts of the transverse current (J_y) are even-symmetric and have maximum values on the central plane. Fig. 8(b) illustrates the transverse and longitudinal modal currents on the ground plane of the EME microstrip at 12.35 GHz. Currents are normalized to a maximum of unity. Real and imaginary parts of the longitudinal current (J_x) are odd-symmetric and real and imaginary parts of the transverse current (J_y) are even-symmetric. In both

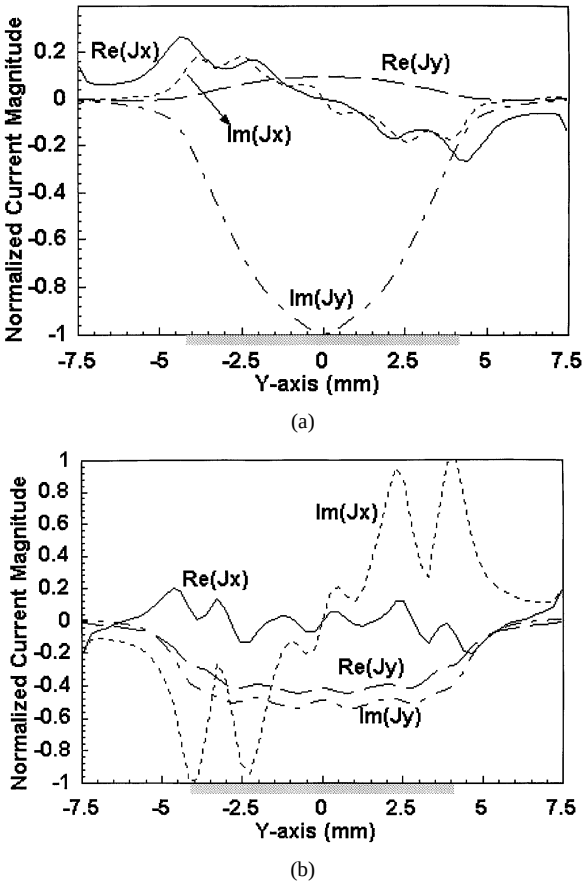

Fig. 8. Normalized current distribution of the higher order leaky modes for the EME microstrip. The metal strip of the EME microstrip is located from $y = -4.268$ mm to $y = 4.268$ mm. (a) At 5.25 GHz with the normalized propagation constant $\gamma/k_0 = 0.06 + j0.67$. (b) At 12.35 GHz with $\gamma/k_0 = 0.13 + j0.64$.

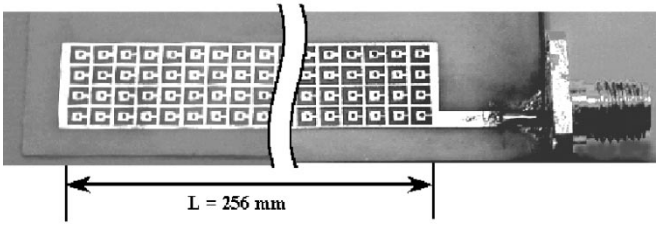

Fig. 9. Photograph of the dual-frequency EME microstrip leaky-mode antenna.

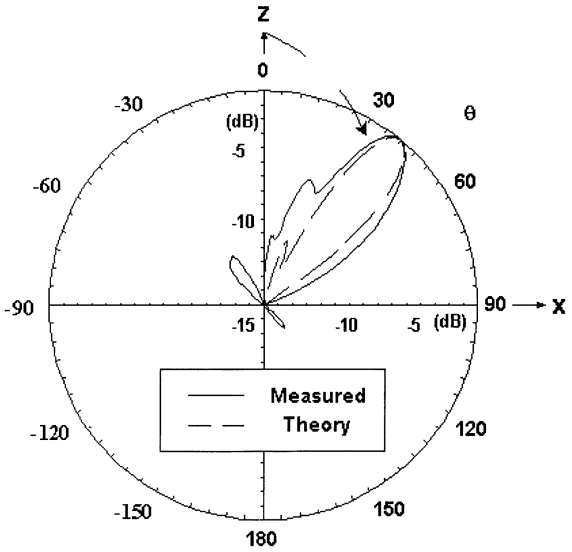

Fig. 10. Theoretical and measured far-field H-plane radiation patterns of the asymmetrically-fed EME microstrip leaky-mode antenna at 5.25 GHz. θ presents the tilt angle of the main beam from the broadside direction.

leaky regions, the longitudinal currents (J_x) are odd-symmetric and the transverse currents (J_y) are even-symmetric. The current vectors on the ground plane of the EME microstrip antenna are primarily transverse to the direction of the waves that propagate along the EME microstrip, consistent with the first higher order EH_1 leaky mode of the uniform microstrip. Therefore, the leaky-wave characteristics of the EME microstrip antenna at both bands are similar to those of a uniform microstrip at a higher order EH_1 mode.

C. Measurements

A dual-frequency EME microstrip leaky-mode antenna is fabricated and tested based on the theoretical analyses outlined in the previous subsection. The experimental antenna is fed asymmetrically with a 50-Ω microstrip 1.6-mm wide ($W_p = 1.6$ mm) and 0.5-mm long ($L_p = 0.5$ mm). The antenna has the same dimensions as that in Fig. 1(a) with a length of 256 mm ($L = 256$ mm) and a width of 8.536 mm ($W = W_M = 8.536$ mm). The length of the EME microstrip is 4.5 λ_0 (free-space wavelength at 5.25 GHz) and exceeds the required 3.9 λ_0 if more than 90% of the electromagnetic energy leaks [24]. Fig. 9 displays a photograph of the dual-frequency EME microstrip leaky-mode antenna, showing a typical asymmetric feed reported by Menzel [25]. The asymmetric feed for an exciting leaky EH_1 microstrip mode has been a well-known technique.

The H-plane (the x–z-plane) radiation pattern measurement is obtained in an anechoic chamber. The two radiation bands, from 5.05 to 5.45 GHz and from 11.95 to 13.0 GHz, are observed. Outside the space-wave leaky region, the radiation pattern contains several lobes and nulls. The far-field theoretical radiation pattern is obtained by invoking the full-wave integral equation solver IE3D. Fig. 10 shows that the theoretical and measured co-polarization far-field patterns along the H-plane agree closely at 5.25 GHz. The difference between the two main beam angles is under 1.5° and the measured beamwidth is slightly greater than the theoretical prediction. Fig. 11(a) and (b) depict the far-field radiation patterns of the EME microstrip antenna at two radiation regions. In the first radiation band, the tilt angle of the main beam increases from 26° to 56°, as the operating frequency increases from 5.15 to 5.35 GHz. The tilt angle increases from 25° to 63° in the second radiation band as the frequency increases from 12.15 to 12.75 GHz. The frequency-scanning properties of the EME microstrip antenna are similar to those of the uniform microstrip leaky-wave antenna. Additionally, radiation beam with the same tilt angle can be obtained in two radiation regions; for example, the radiation angles are approximately 39° at both 5.25 and 12.35 GHz. The measured 3-dB beamwidth is 19° at 5.25 GHz, which is slightly greater than 14.5° at 12.35 GHz.

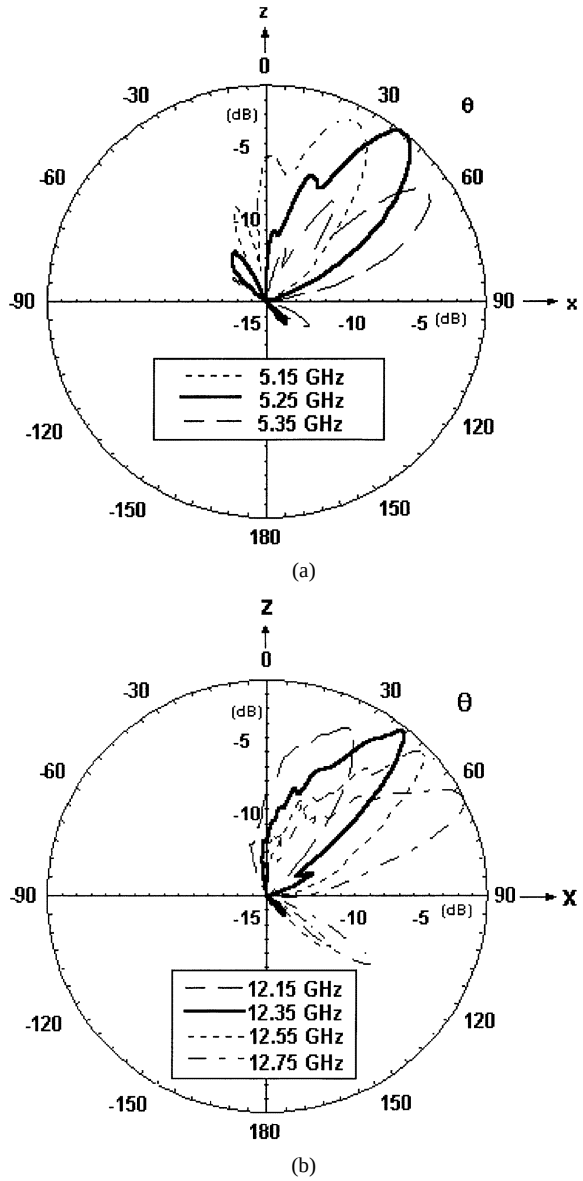

Fig. 11. Frequency-scanning H-plane radiation patterns of the EME microstrip dual-frequency antenna. (a) First radiation region. (b) Second radiation region.

The normalized phase constant β/k_0 of the higher order mode is related to the angle θ_m of the leakage by $\theta_m \approx \sin^{-1}(\beta/k_0)$, where k_0 is the free-space wavenumber and the main beam angle θ_m is measured from the broadside direction (z axis) [26]. The measured value of the main beam angle θ_m at two radiation regions are converted to the normalized phase constants (β/k_0) which are superimposed on the normalized phase constant curve in Fig. 7, demonstrating the excellent agreement of normalized phase constants obtained by two theoretical methods and measurement.

IV. Conclusion

Substituting the PBG structure for a uniform metal strip of a conventional microstrip adds more degrees of freedom to the design of new guided-wave structure such as the so-called EME microstrip. Mingling the modal properties of the first (TM) mode and the second (TEM) mode of the PBG MS to the EME microstrip, the leaky properties of the conventional, uniform microstrip are greatly transformed, resulting in dual-band leaky modes, which in many aspects resemble the leaky EH_1 mode of a conventional microstrip. Both theoretical analyses and experimental results show excellent agreement for the dispersion curve of the EME microstrip, confirming the dual-frequency operation of two leaky EH_1-like modes of the EME microstrip.

References

[1] E. Yablonovitch, "Photonic band-gap structures," *J. Opt. Soc. Amer. B, Opt. Phys.*, vol. 10, no. 2, pp. 283–295, Feb. 1993.

[2] J. D. Joannopoulos, R. D. Meade, and J. N. Winn, *Photonic Crystals: Modeling the Flow of Light*. Princeton, NJ: Princeton Univ. Press, 1995.

[3] I. El-Kady, M. M. Sigalas, R. Biswas, and K. M. Ho, "Dielectric waveguides in two-dimensional photonic bandgap materials," *J. Lightwave Technol.*, vol. 17, pp. 2042–2049, Nov. 1999.

[4] S. T. Peng and R. B. Hwang, "Analysis of two-dimensionally periodic structures graphical methods and physical consequences," in *Proc. 29th Eur. Microwave Conf.*, Munich, Germany, 1999, pp. 299–302.

[5] D. Sievenpiper, L. Zhang, R. F. J. Broas, N. G. Alexopolous, and E. Yablonovitch, "High-impedance electromagnetic surfaces with a forbidden frequency band," *IEEE Trans. Microwave Theory Tech.*, vol. 47, pp. 2059–2074, Nov. 1999.

[6] F. R. Yang, K. P. Ma, Y. Qian, and T. Itoh, "A novel TEM waveguide using uniplanar compact photonic-bandgap (UC-PBG) structure," *IEEE Trans. Microwave Theory Tech.*, vol. 47, pp. 2092–2098, Nov. 1999.

[7] ——, "A uniplanar compact photonic-bandgap (UC-PBG) structure and its applications for microwave circuit," *IEEE Trans. Microwave Theory Tech.*, vol. 47, pp. 1509–1514, Aug. 1999.

[8] R. Coccioli, F. R. Yang, K. P. Ma, and T. Itoh, "Aperture-coupled patch antenna on UC-PBG substrate," *IEEE Trans. Microwave Theory Tech.*, vol. 47, pp. 2123–2130, Nov. 1999.

[9] C. K. Wu, H. S. Wu, and C. K. Tzuang, "Electric-magnetic-electric (EME) slow-wave microstrip line and bandpass filter of compressed size," *IEEE Trans. Microwave Theory Tech.*, vol. 50, pp. 1996–2004, Aug. 2002.

[10] C. K. Wu and C. K. Tzuang, "Slow-wave propagation of microstrip consisting of electric-magnetic-electric (EME) composite metal strips," in *IEEE MTT-S Int. Microwave Symp. Dig.*, Phoenix, AZ, May 20–25, 2001, pp. 727–730.

[11] ——, "Dispersion characteristics of EME microstrip at first higher order," in *IEEE MTT-S Int. Microwave Symp. Dig.*, Seattle, WA, June 2–7, 2002, pp. 1083–1086.

[12] H. Y. D. Yang, N. G. Alexopoulos, and E. Yablonovitch, "Photonic band-gap materials for high-gain printed circuit antennas," *IEEE. Trans. Antennas Propagat.*, vol. 45, pp. 185–187, Jan. 1997.

[13] H. Y. D. Yang, R. Kim, and D. R. Jackson, "Design consideration for modeless integrated circuit substrates using planar periodic patches," *IEEE Trans. Microwave Theory Tech.*, vol. 48, pp. 2233–2239, Dec. 2000.

[14] T. K. Wu, Ed., *Frequency Selective Surface and Grid Array*. New York: Wiley, 1995.

[15] W. J. Chappell, M. P. Little, and L. P. B. Katehi, "High Q two dimensional defect resonators – measured and simulated," in *IEEE MTT-S Int. Microwave Symp. Dig.*, Jun. 2000, pp. 143–1440.

[16] S. D. Chen and C. K. Tzuang, "Characteristic impedance and propagation of the first higher-order microstrip mode in frequency and time domain," *IEEE Trans. Microwave Theory Tech.*, vol. 50, pp. 1370–1379, May 2002.

[17] H. K. Smith and P. E. Mayes, "Log-periodic array of dual-feed microstrip patch antennas," *IEEE Trans. Antennas Propagat.*, vol. 39, pp. 1659–1664, Dec. 1991.

[18] H. S. Wu, C. K. Tzuang, and K. C. Chen, "Simultaneous suppression and enhancement of crosstalk of microstrip discontinuities by periodical lattice structure," in *Proc. Int. Signal, Syst., Electron. Symp.*, Tokyo, Japan, July 24–27, 2001, pp. 730–737.

[19] C. K. Tzuang and Y. C. Chen, "Dispersion characteristics of microstrip with periodic perturbations," in *IEEE MTT-S Int. Microwave Symp. Dig.*, Boston, MA, June 11–16, 2000, pp. 1537–1540.

[20] Y. C. Chen and C. K. Tzuang, "Fields and waves in microstrip on uniplanar compact photonic-bandgap (UC-PBG) ground plane," in *Proc. 31th Eur. Microwave Conf.*, vol. 2, London, U.K., Sep. 24–28, 2001, pp. 177–180.

[21] ——, "Dispersion characteristics of microstrip on uniplanar compact photonic-bandgap (UC-PBG) ground plane and electric-magnetic-electric (EME) microstrips," in *Proc. Asia–Pacific Microwave Conf.*, vol. 2, Taipei, Taiwan, R.O.C., Dec. 3–6, 2001, pp. 779–782.
[22] R. S. Adve, T. K. Sarkar, O. M. C. Pereira-Filho, and S. M. Rao, "Extrapolation of time-domain responses from three-dimensional conducting objects utilizing the matrix pencil technique," *IEEE Trans. Antennas Propagat.*, vol. 45, pp. 147–156, Jan. 1997.
[23] Y. Hua and T. K. Sarkar, "Generalized pencil-of-function method for extracting poles of EM system from its transient response," *IEEE Trans. Antennas Propagat.*, vol. 37, pp. 229–234, Feb. 1989.
[24] A. A. Oliner, "Leakage from higher modes on microstrip line with application t antennas," *Radio Sci.*, vol. 22, no. 6, pp. 907–912, Nov. 1987.
[25] W. Menzel, "A new traveling-wave antenna in microstrip," *Arch. Electron. Uebertrag. Tech.*, vol. 33, pp. 137–140, Apr. 1979.
[26] G. J. Chou and C. K. Tzuang, "Oscillator-type active-integrated antenna: The leaky-mode approach," *IEEE Trans. Microwave Theory Tech.*, vol. 44, pp. 2265–2272, Dec. 1996.

Yu-Chiao Chen (S'99) was born in Tainan, Taiwan, R.O.C., in 1975. He received the B.S. and M.S. degrees in communication engineering from the National Chiao Tung University, Hsinchu, Taiwan, R.O.C., in 1998 and 2000, respectively, and is currently working toward the Ph.D. degree in communication engineering at the same university.

His current research interests include field theory analysis and application designing of periodic structures.

Ching-Kuo Wu (S'99) was born in Changhua, Taiwan, R.O.C., in 1971. He received the B.S. degree in electrical engineering from the National Cheng Kung University, Tainan, Taiwan, R.O.C., in 1993, the M.S. degree in communication engineering from the National Chiao Tung University, Hsinchu, Taiwan, R.O.C., in 1995, and is currently working toward the Ph.D. degree in communication engineering at National Chiao Tung University.

From 1997 to 1998, he was with the Computer and Communication Laboratories, Industrial Technology Research Institute, Hsinchu, Taiwan, R.O.C., where he was involved with the development of RF modules for a GSM/DCS1800 handset. His current research interests include the analysis and design of microwave and millimeter-wave components and PBG structures.

Ching-Kuang C. Tzuang (S'80–M'80–SM'92–F'99) received the B.S. degree in electronic engineering from the National Chiao Tung University, Hsinchu, Taiwan, R.O.C., in 1977, the M.S. degree from the University of California at Los Angeles, in 1980, and the Ph.D. degree in electrical engineering from the University of Texas at Austin, in 1986.

From 1981 to 1984, he was with TRW, Redondo Beach, CA, where he was involved with analog and digital MMICs. Since 1986, he has been with the Institute of Communication Engineering, National Chiao Tung University. His research activities involve the design and development of millimeter-wave and microwave active and passive circuits and the field theory analysis and design of various complex waveguiding structures and large-array antennas. He has supervised 58 M.S. students and 15 Ph.D. students.

Dr. Tzuang helped in the formation of the IEEE Microwave Theory and Techniques Society (IEEE MTT-S) Taipei chapter, and served as secretary, vice chairman, and chairman in 1988, 1989, and 1990, respectively. He has been on the Asia–Pacific Microwave Conference International Steering Committee, where, since 1994, he has represented the Taipei chapter as the international liaison officer.